IEEE Access
Multidisciplinary | Rapid Review | Open Access Journal

Received February 9, 2020, accepted February 24, 2020, date of publication February 27, 2020, date of current version March 10, 2020.

Digital Object Identifier 10.1109/ACCESS.2020.2976779

Modeling and Identification of Temperature-Dependent Hysteresis in Piezoelectric Materials Considering Parameter Sensitivity

YANFANG LIU[1], NAIMING QI[1], AND ZHI LI[2]
[1]School of Astronautics, Harbin Institute of Technology, Harbin 150001, China
[2]State Key Laboratory of Synthetical Automation for Process Industries, Northeastern University, Shenyang 110819, China

Corresponding author: Yanfang Liu (liu-yanfang@hotmail.com)

This work was supported in part by the National Natural Science Foundation of China under Grant 51705109, Grant U1737207, and Grant 11672093, in part by the Startup Fund for Heilongjiang Postdoctoral under Grant LBH-Q19102, in part by the Innovation Fund from Shanghai Academy of Spaceight Technology under Grant AST-2018-109, and in part by "2511" First Class High Level Discipline Direction Construction Project.

ABSTRACT Hysteresis is an important nonlinearity effect in piezoelectric materials and is sensitive to temperature. This paper extends the saturated capacitor model to capture temperature-dependent hysteresis by replacing the constant parameters with functions of temperature. To obtain these functions, several sets of constant parameters are identified at different temperatures, and then each term of the parameters is fitted as a function with respect to temperature. In the curve fitting process, the parameter sensitivity is employed as a weight factor. The effectiveness of the proposed modeling and parameter determination procedure is verified with experimental data. The overall normalized root mean square error is approximately 5%, including 3% error caused by the identified parameters.

INDEX TERMS Temperature-dependent hysteresis, modeling and identification, piezoelectric materials, saturated capacitor hysteresis model.

I. INTRODUCTION

Despite their advantages such as high stiffness and fast response, piezoelectric materials also possess some disadvantages, namely, hysteresis, creep, radiation effects, and temperature effect [1], [2]. Hysteresis is generally considered to be a memory effect in which the output displacement depends on a combination of the currently applied voltage and on some past values of the applied voltage. Creep is a slow drift in the displacement that follows the rapid response to a sudden change in the input voltage. Hysteresis and creep together can lead to inaccuracy in open-loop control and instability in closed-loop control.

Some approaches to handle hysteresis and/or creep include improving the material [3], charge-driven approach [1], [4], [5], modeling and compensation (M&C) [6], [7], and the feedback technique [8]–[10]. Among these approaches, the M&C approach is one of the most effective ways to handle hysteresis and creep and has attracted considerable attention. This approach obtains linear performance by modeling and compensating the nonlinearities. Meanwhile, the feedback technique can also be applied to the compensated system to enhance the performance [8], [11]–[13]. The Preisach [14]–[16] and Prandtl-Ishlinskii models [17]–[20] are widely used to model hysteresis in piezoelectric materials. These models belong to the class of operators with a Preisach memory and are essentially a mathematical description of observed hysteresis. The saturated capacitor hysteresis (SCH) model [21]–[24] is another popular hysteresis model. The SCH model has physical significance in both the mechanical and electrical domains. These hysteresis models are quasi-static. To address the rate-dependent feature caused by creep, linear time-invariant [19], logarithmic [20], [25], [26], and fractional-order [23], [27] models have been proposed to model the creep and introduced into the hysteresis model.

However, the above works mainly focus on the hysteresis and creep phenomena at room temperature, which are assumed to be constant. Unfortunately, the performance

The associate editor coordinating the review of this manuscript and approving it for publication was Giambattista Gruosso.

of piezoelectric materials is quite sensitive to temperature. Changes in temperature result in expansion of the piezoelectric material and influence the material's parameters [28]. The former is referred to as the thermomechanical effect, and the latter causes the nonlinearities of hysteresis and creep to be temperature-dependent [29]–[31]. The thermomechanical effect is simple and well studied. This effect can be compensated for in the forward loop or even utilized to design a hybrid actuator [32]. The effect of temperature on creep is significant. Fortunately, creep is quite slow, and thus, operating a piezoelectric actuator (PEA) fast enough can help reduce the drift caused by creep. Meanwhile, creep can be weakened by properly initializing the PEA [23]. The feedback technique can also be utilized to remove the creep effect [28], [33]. The effect of temperature on hysteresis is weak if the temperature varies in a small range [28], [33] and becomes obvious if the temperature changes in a wide range [29], [31], [34]. The hysteresis shape and the slope of hysteresis curves clearly change and should be investigated.

Controlling the environment temperatures can manage the temperature effect. However, it is quite difficult or expensive to control the environment in some situations, such as in outer space. Meanwhile, self-heating may also cause the temperature of the PEA to change. In [32], the author proposed a hybrid thermopiezoelectric microactuator utilizing the thermomechanical effect. However, the coupling effect between the hysteresis and temperature was not given. In [28], [33], the thermal expansion is modeled, and the effect of temperature on creep is rejected by the closed-loop controller. However, the effect of temperature on hysteresis is neglected. A modified Preisach operator was proposed in [34] by directly including the temperature dependence in the Preisach operator. In [29], a more complete model was presented. However, in the above works, the temperature influence is mainly on the slope of the hysteresis curves. Thus, the temperature-dependent Preisach density function is almost linear with respect to temperature. If the temperature varies in a wide range, both the slope of hysteresis curves [29], [34] and the hysteresis shape are changed.

The contribution of this paper is extending the SCH model into a temperature dependent model. The SCH model is generalized to be able to capture non-convex hysteresis, and then, it is expanded to capture temperature-dependent hysteresis by replacing the constant parameters of the SCH model by temperature-dependent ones. A detailed parameter determination procedure is also provided, in which the parameter sensitivity are taken into consideration. Based on experimental data, the effectiveness of the proposed model and procedure are demonstrated. Results show that the proposed approach guarantees a sufficient precision for a wide temperature range.

II. PHYSICAL MODEL

A. SCH MODEL

The SCH model consists of several saturated capacitors (SCs) that are connected in series, as shown in Fig. 1. The

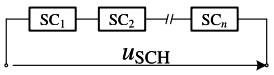

FIGURE 1. The SCH model.

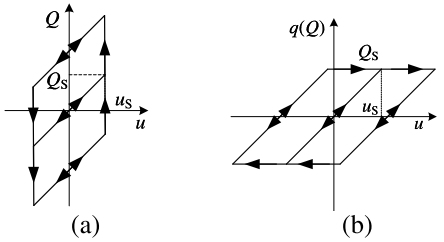

FIGURE 2. The charge-voltage property of (a) the original SC and (b) the new type of SC.

charge-voltage property of an SC is shown in Fig. 2(a). Before the capacitor is saturated, the SC performs like an ideal capacitor. The charge increases linearly with voltage, u, applied on it. The charge input, denoted as Q, equals the charge stored on it, denoted as q. Once q is saturated, q and u reach and remain at the saturation values Q_S and u_S, respectively. The charge input Q increases as the SC performs like a wire. The SCH model is governed by

$$\dot{q}_i = \begin{cases} \dot{Q} & |q_i| < Q_{S,i} \\ 0 & |q_i| \geq Q_{S,i} \end{cases} \tag{1}$$

$$q_i = C_i u_i, \quad C_i \in \mathbb{R}^+ \tag{2}$$

$$u_{SCH} = \sum_{i=1}^{n} u_i \tag{3}$$

where C_i, u_i, q_i, and $Q_{S,i}$ are the capacitance, the applied voltage, the stored charge, and the saturation charge of the i-th SC, respectively. The symbol u_{SCH} represents the voltage applied to the networks. To avoid the SCH model becoming saturated, the last SC has a sufficiently large saturation charge and never saturates. Due to the serial connection, the charge input to the SCH model equals the charge stored on the last SC, namely, $Q = q_n$.

The original SCH model can only capture convex hysteresis. The reason is explained in the Appendix. To overcome this limitation, the SCH model is generalized in the following subsection.

B. GENERALIZATION OF THE SCH MODEL

As illustrated in Fig. 3(a), a piece of piezoelectric material consists of a vast amount of Weiss domains, as observed under a microscope. Under an applied electric field, the polarization of a Weiss domain causes its capacitance to increase or decrease, as shown in Fig. 3(b). The capacitance change is simply assumed to be a piecewise linear switch. The capacitance increase switch (Fig. 4(a)) is equalized by the serial connection of an ideal capacitor and an SC (Fig. 4(c)). The capacitance decrease switch (Fig. 4(b)) is equalized by

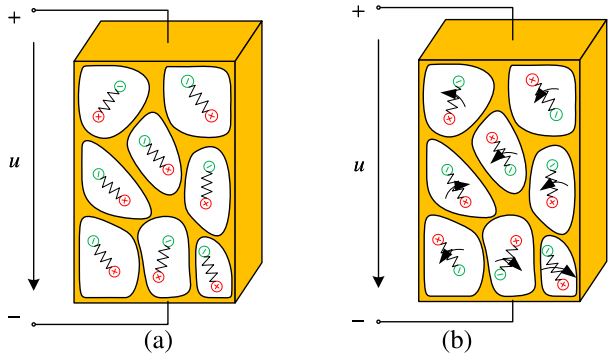

FIGURE 3. Illustration of Weiss domain behavior: (a) under a given voltage and (b) as the voltage increases.

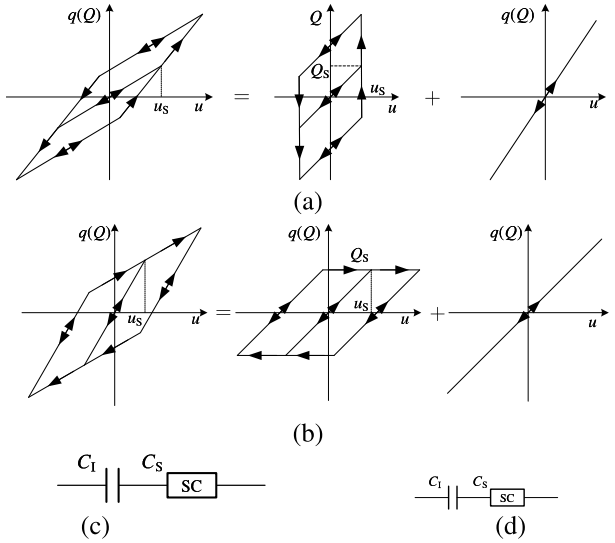

FIGURE 4. Capacitance change of Weiss domain and equivalent circuit: (a) capacitance increase switch, (b) capacitance decrease switch, equivalent circuit for (c) capacitance increase switch, and for (d) capacitance decrease switch.

the parallel connection of an ideal capacitor and another type of SC (Fig. 4(d)).

The charge-voltage property of the new type of SC is shown in Fig. 2(b). Similarly, before the SC is saturated, the SC performs as an ideal capacitor. The charge increases linearly with the applied voltage u. However, once it is saturated, it performs as an ideal insulator. The charge remains at Q_S, and the voltage can increase to any value that is larger than u_S.

The parallel connected network in Fig. 4(d) can be equalized by a serially connected network in Fig. 4(c). The equivalent capacitance C_S is obtained as

$$C_S = -\frac{C_I^2}{C_P} - C_I \tag{4}$$

where C_I and C_P are the capacitances of the ideal capacitor and the new type of SC, respectively. Since $C_I, C_P > 0$, then $C_S < 0$, namely, the equivalent capacitance is negative. Then,

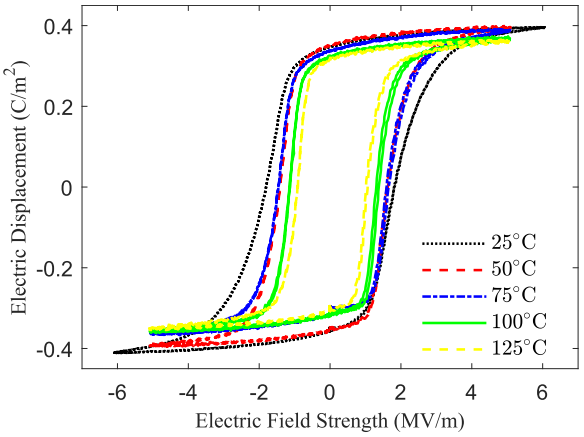

FIGURE 5. The temperature-dependent hysteresis loops [31].

the SCH model can be generalized by removing the constraint $C_i \in \mathbb{R}^+$ in (2).

C. TEMPERATURE-DEPENDENT SCH MODEL

The hysteresis loops under different temperatures are obtained experimentally and are shown in Fig. 5. As the temperature increases, the hysteresis loops become narrow, and the changes in slope become obvious. However, because the capacitance C_i is constant, the above model can only capture temperature-independent hysteresis. In fact, rather than being a constant, the capacitance of ceramics varies with temperature. To overcome this limitation, constant capacitances are replaced by temperature-dependent ones, namely, capacitances are functions of temperature. The temperature-dependent SCH model is expressed as

$$\dot{q}_i = \begin{cases} \dot{Q} & |q_i| < Q_{S,i}(T) \\ 0 & |q_i| \geq Q_{S,i}(T) \end{cases} \tag{5}$$

$$q_i = C_i(T)u_i \tag{6}$$

$$u_{SCH} = \sum_{i=1}^{n} u_i \tag{7}$$

where $Q_{S,i}(T)$ and $C_i(T)$ are functions of saturation charge and capacitance, respectively.

III. IDENTIFICATION PROCEDURE

A. PARAMETER IDENTIFICATION PROBLEM

The hysteresis property is solely governed by $Q_{S,i}(T)$ and $C_i(T)$, which are obtained by solving the minimization problem

$$\min_{\substack{C_i(T), i=1,\ldots,n \\ Q_{S,i}(T), i=1,\ldots,n-1}} \sqrt{\frac{1}{N}\sum_{k=1}^{N}[Q(t_k) - \mathrm{SCH}[u](t_k)]^2} \tag{8}$$

where SCH denotes the SCH model and N is the number of samples.

It is difficult to identify these functions directly. To simplify the identification procedure, $Q_{S,i}(T_j)$ for a fixed T_j and $i \in \{1, 2, \ldots, n\}$ are assumed to follow a given distribution.

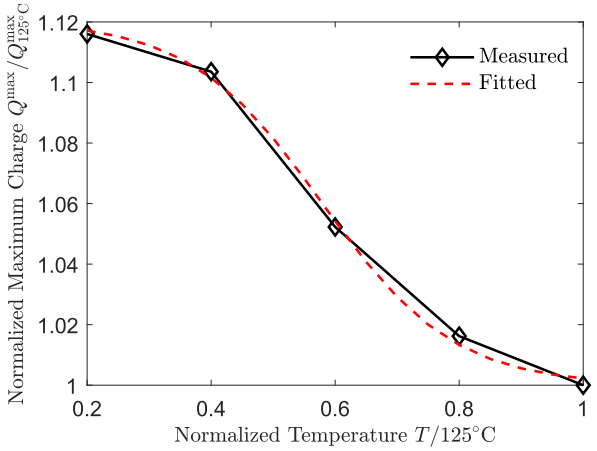

FIGURE 6. The relationship between the maximum charge and temperature.

Meanwhile, $Q_{\mathrm{S},i}(T)$ for different SCs are assumed to have similar shapes. Then, $Q_{\mathrm{S},i}(T)$ is determined directly, and the above problem is simplified as

$$\min_{C_i(T),i=1,\ldots,n} \sqrt{\frac{1}{N}\sum_{k=1}^{N}[Q(t_k)-\mathrm{SCH}[u](t_k)]^2} \tag{9}$$

To determine $C_i(T)$, its values are identified at several given temperatures T_j, and then the map $T \mapsto C_i$ is fitted to be a function.

B. DETERMINATION OF FUNCTIONS OF SATURATION CHARGE

The charge Q is obtained by multiplying the electric displacement by the area. Its maximum value $Q^{\max}$ is normalized by that at a temperature of 125°C, i.e., $Q^{\max}_{125°C}$, and plotted in Fig. 6. The expression of $\overline{Q}^{\max}(T)$ is selected as

$$\overline{Q}^{\max}(T) = \frac{k_1 + k_2 \mathrm{e}^{k_3 \overline{T}}}{1 + k_2 \mathrm{e}^{k_3 \overline{T}}} \tag{10}$$

where $\overline{Q}^{\max}(T) = Q^{\max}(T)/Q^{\max}_{125°C}$ and $\overline{T} = T/125°C$. The identified parameters are $k_1 = 1.1205$, $k_2 = 4.2941 \times 10^{-1}$, and $k_3 = 9.4193$. As shown in Fig. 6, the fitted result closely follows the experimental values.

As shown in Fig. 5, the switch of the slope has a 'fast-slow-fast' manner. The slope changes once an SC is saturated. Thus, more SCs with relatively small and relatively large saturation charges are required. The distribution of $Q_{\mathrm{S},i}(T)$ is selected as

$$Q_{\mathrm{S},i}(T) = Q^{\max}(T)\frac{\arctan(-s+i\mathrm{d}s)+\arctan(s)}{2\arctan(s)} \tag{11}$$

where s is a parameter used to determine the distribution density and $\mathrm{d}s = 2s/n$. Then,

$$Q_{\mathrm{S},i}(T) = Q^{\max}_{125°C}\frac{k_1 + k_2 \mathrm{e}^{k_3 \overline{T}}}{1 + k_2 \mathrm{e}^{k_3 \overline{T}}}\frac{\arctan(-s+i\mathrm{d}s)+\arctan(s)}{2\arctan(s)} \tag{12}$$

TABLE 1. Saturation charges for different temperatures.

i	$Q_{\mathrm{S},i}$ (μC)				
	25°C	50°C	75°C	100°C	125°C
1	1.78E-2	1.76E-2	1.68E-2	1.62E-2	1.60E-2
2	4.06E-2	4.00E-2	3.83E-2	3.68E-2	3.64E-2
3	6.98E-2	6.88E-2	6.59E-2	6.33E-2	6.26E-2
4	1.07E-1	1.05E-1	1.01E-1	9.69E-2	9.58E-2
5	1.52E-1	1.50E-1	1.43E-1	1.38E-1	1.36E-1
6	2.02E-1	1.99E-1	1.91E-1	1.83E-1	1.81E-1
7	2.53E-1	2.49E-1	2.38E-1	2.29E-1	2.27E-1
8	2.98E-1	2.93E-1	2.81E-1	2.70E-1	2.67E-1
9	3.35E-1	3.30E-1	3.16E-1	3.03E-1	3.00E-1
10	3.64E-1	3.59E-1	3.43E-1	3.30E-1	3.26E-1
11	3.87E-1	3.81E-1	3.65E-1	3.51E-1	3.47E-1

The saturation charge of the last SC, $Q_{\mathrm{S},n}(T)$, is replaced by a sufficiently large value to avoid saturation of the SCH model. In this paper, $n = 12$, and $s = 1.5$. Then, the saturation charges are obtained, as presented in Table 1.

C. IDENTIFICATION OF FUNCTIONS OF CAPACITANCE

The capacitances $C_i(T_j)$ are identified by solving

$$\min_{C_i(T_j),i=1,\ldots,n} \sqrt{\frac{1}{N_j}\sum_{k=1}^{N_j}\left[Q_j(t_k)-\mathrm{SCH}[u_j](t_k)\right]^2} \tag{13}$$

with the initial parameters obtained from the increasing curve of the hysteresis [22]–[24]. The identified results are shown in Fig. 7 with two magnified figures for the first 3 and last 4 SCs, respectively. Generally, the parameters have the same trends for different temperatures. This result is not difficult to understand because the hysteresis loops have similar shapes. The first 5 SCs, as well as the last one, have positive capacitances, whereas the others have negative values. The absolute values for the first 3 and last 4 SCs are extremely small.

The capacitance $C_i(T)$ is simply treated as an m-order polynomial function of temperature

$$C_i(T) = \sum_{j=0}^{m} a_{i,j}\overline{T}^j \tag{14}$$

Then, the optimal coefficients are obtained as

$$\boldsymbol{a}_i = (\boldsymbol{A}_i^{\mathrm{T}}\boldsymbol{A}_i)^{-1}\boldsymbol{A}_i^{\mathrm{T}}\boldsymbol{C}_i \tag{15}$$

where $\boldsymbol{C}_i = [C_i(T_1), C_i(T_2), \cdots, C_i(T_M)]^{\mathrm{T}}$, $\boldsymbol{a}_i = [a_{i,0}, a_{i,1}, \cdots, a_{i,m}]^{\mathrm{T}}$ and

$$\boldsymbol{A}_i = \begin{bmatrix} 1 & T_1 & T_1^2 & \cdots & T_1^m \\ 1 & T_2 & T_2^2 & \cdots & T_2^m \\ \vdots & \vdots & \vdots & \ddots & \vdots \\ 1 & T_M & T_M^2 & \cdots & T_M^m \end{bmatrix}$$

In (15), all the parameters are treated with the same weight. In practice, different parameters may have different effects on the results. The parameter sensitivity, representing the

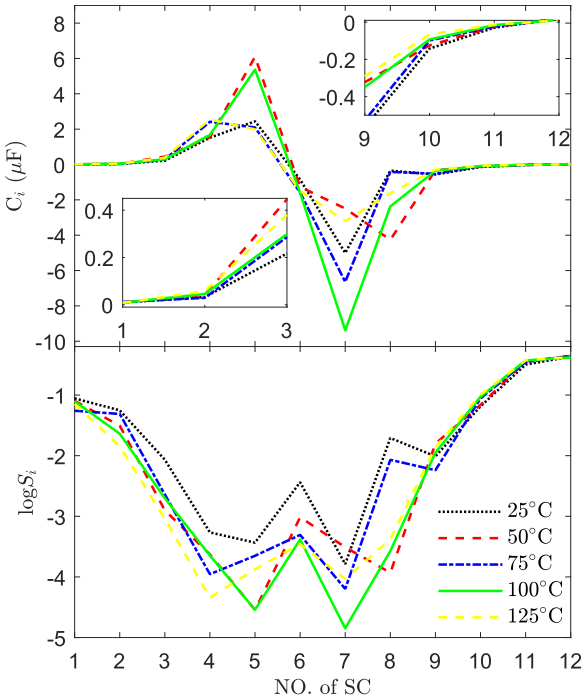

FIGURE 7. The identified capacitances and parameter sensitivity.

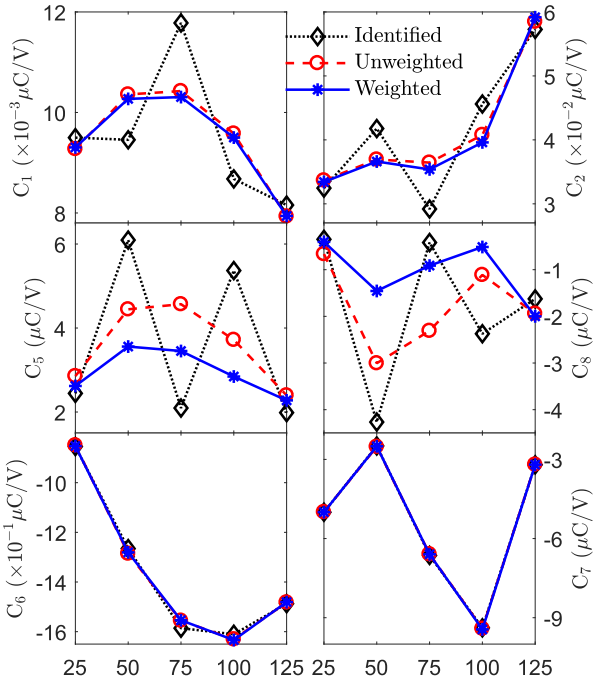

FIGURE 8. The optimized capacitance functions.

increase in modeling error caused by the change in the parameter's value, is defined as

$$S_i(T_j) = \left|\frac{\mathrm{d}e_{\mathrm{NRMS}}}{\mathrm{d}C_i(T_j)}\right| = \left|\frac{\Delta e_{\mathrm{NRMS}}}{\Delta C_i(T_j)}\right| \tag{16}$$

where e_{NRMS} is the normalized root mean square (NRMS) error

$$e_{\mathrm{NRMS}} = \frac{1}{Q^{\max}_{125^\circ\mathrm{C}}}\sqrt{\frac{1}{N_j}\sum_{k=1}^{N_j}\left[Q_j(t_k) - \mathrm{SCH}[u_j](t_k)\right]^2} \tag{17}$$

The parameter sensitivity is further normalized by

$$\overline{S}_i(T_j) = \frac{S_i(T_j)}{\sum_{i=1}^{n} S_i(T_j)} \tag{18}$$

As shown in Fig. 7, the capacitances of the first 3 and last 4 SCs are small, but the modeling error is quite sensitive to them, especially for the first 2 and last 3 SCs.

A parameter with a larger sensitivity should have a larger weight factor as the modeling error is more sensitive to it. Thus, (15) is modified as

$$\boldsymbol{a}_i = (\boldsymbol{A}_i^{\mathrm{T}}\boldsymbol{W}_i\boldsymbol{A}_i)^{-1}\boldsymbol{A}_i^{\mathrm{T}}\boldsymbol{W}_i\boldsymbol{C}_i \tag{19}$$

where

$$\boldsymbol{W}_i = \sqrt{\mathrm{diag}([\overline{S}_i(T_1), \overline{S}_i(T_2), \cdots, \overline{S}_i(T_n)]^{\mathrm{T}})} \tag{20}$$

The data are obtained at five different temperatures, and 3-order polynomials are utilized, i.e., $m = 3$ and $M = 5$. The coefficients are obtained and, then, the capacitances are calculated. Some typical results are shown in Fig. 8. The 3-order polynomial is capable of fitting curves $C_6 - T$ and $C_7 - T$. It does not fit curves $C_1 - T$, $C_2 - T$, $C_5 - T$, and $C_8 - T$ well. But as it is demonstrated in the next section, the poor fitting results does not have obvious effect on the model precision. From the result of $C_1 - T$, for the weighted optimization results, the errors at temperatures 50°C and 100°C are smaller, but that at 75°C is greater. The reason for this result is that the sensitivity at temperature 75°C is smaller. Similar phenomena are more obvious for $C_2 - T$, $C_5 - T$, and $C_8 - T$.

IV. EVALUATION AND DISCUSSION

Experimental data are used to verify the proposed model. The maximum charge at 125°C, $Q^{\max}_{125^\circ\mathrm{C}}$, is employed as a reference value. Then, $Q^{\max}(T)$ are obtained by (10). Select $n = 12$ and $s = 1.5$. Then, $Q_{\mathrm{S},i}(T)$ is given by (12) and a capacitance of a 3-order polynomial function of temperature are obtained. The simulated results of (5) are compared with the experimental data in Fig. 9. The results obtained by using the identified parameters are also plotted in these figures.

The identified results follow the experiment closely, which indicates that the generalized SCH model has the capability to capture concave and convex hysteresis at a constant temperature. Although the 3-order polynomial function is not very suitable for fitting the capacitance-temperature curve, the results using coefficients with sensitivity-weighted show an acceptable precision. The NRMS errors are presented in Table 2. The error of the identified results is less than 5%, approximately 3%, while the error of the results generated using parameters without sensitivity-weighted is approximately 10%. The error with sensitivity-weighted is much

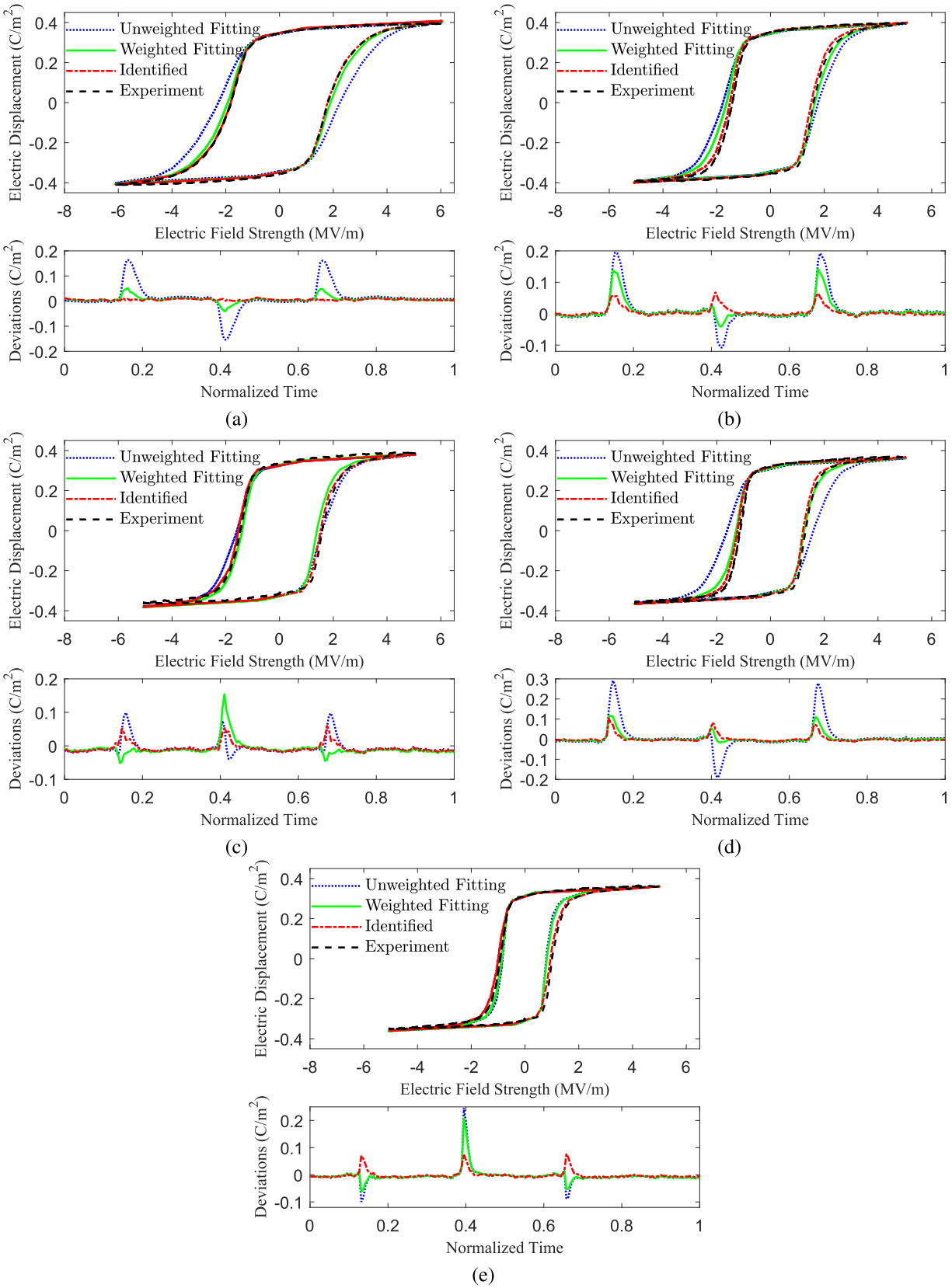

FIGURE 9. Comparison between the simulated results and experimental data: (a) $T = 25°C$, (b) $T = 50°C$, (c) $T = 75°C$, (d) $T = 100°C$, and (e) $T = 125°C$.

TABLE 2. Modeling errors.

Temperature (°C)	Identified	Unweighted	Weighted
25	0.70%	9.96%	2.49%
50	3.01%	8.10%	5.10%
75	2.97%	4.17%	4.90%
100	3.57%	12.2%	4.28%
125	3.18%	6.83%	5.77%

smaller, approximately 5%. Considering that the identified parameters lead to errors of approximately 3%, this result demonstrated the superiority of the proposed method.

However, the experimental data was obtained at several constant temperatures but not a time-varying temperature. It is hard to verify the capability of the proposed model on capturing hysteresis behavior under a time-varying temperature.

V. CONCLUSION

In this paper, the SCH model is extended to describe the temperature-dependent feature of the hysteresis in piezoelectric materials. The SCH model is first generalized to capture convex and concave hysteresis. Then, the constant parameters are extended as functions of temperature. The parameter determination procedure is also presented. The effectiveness is verified by experimental data. The identified results contain approximately 3% error. Including this error, the overall error of the proposed model is approximately 5%. Thus, the proposed model and parameter determination procedure are capable of describing the temperature-dependent hysteresis.

APPENDIX

Let n SCs be arranged in the order that the saturation charges increase. Let j be the maximum number where the j-th SC is saturated. The moment before the j-th SC is saturated, the capacitance of the SCH model is

$$C_{\mathrm{SCH}}^{j-} = \frac{1}{\sum_{i=j}^{n} \frac{1}{C_i}} \tag{21}$$

Once the j-th SC is saturated, the capacitance of the SCH model becomes

$$C_{\mathrm{SCH}}^{j+} = \frac{1}{\sum_{i=j+1}^{n} \frac{1}{C_i}} \tag{22}$$

Then, one obtains

$$C_{\mathrm{SCH}}^{j+} - C_{\mathrm{SCH}}^{j-} = \frac{1}{C_j \sum_{i=j}^{n} \frac{1}{C_i} \sum_{i=j+1}^{n} \frac{1}{C_i}} > 0 \tag{23}$$

Thus, the saturation of the j-th SC leads to an increase in the slope of the charge-voltage curve. In other words, the SCH model can only capture convex hysteresis.

REFERENCES

[1] S. Devasia, E. Eleftheriou, and S. O. R. Moheimani, "A survey of control issues in nanopositioning," *IEEE Trans. Control Syst. Technol.*, vol. 15, no. 5, pp. 802–823, Sep. 2007.

[2] P. S. Galvez, S. A. S. Paiva, E. Guillermain, M. Butcher, M. Di Castro, and A. Masi, "Gamma and proton irradiation tests on a piezoelectric actuator," *IEEE Access*, vol. 7, pp. 184398–184410, 2019.

[3] J. Chen and Z. Feng, "X7R dielectric multilayer ceramic capacitors show good micro-actuating properties with little hysteresis," *Electron. Lett.*, vol. 50, no. 7, pp. 538–540, Mar. 2014.

[4] T. Jin, Y. Peng, Z. Xing, and L. Lei, "A charge controller for synchronous linear operation of multiple piezoelectric actuators," *IEEE Access*, vol. 7, pp. 90741–90749, 2019.

[5] S. Rios and A. Fleming, "Design of a charge drive for reducing hysteresis in a piezoelectric bimorph actuator," *IEEE/ASME Trans. Mechatronics*, vol. 21, no. 1, pp. 51–54, Feb. 2016.

[6] I. Ahmad, "Two degree-of-freedom robust digital controller design with Bouc-Wen hysteresis compensator for piezoelectric positioning stage," *IEEE Access*, vol. 6, pp. 17275–17283, 2018.

[7] X. Chen and W. Li, "A monolithic self-sensing precision stage: Design, modeling, calibration, and hysteresis compensation," *IEEE/ASME Trans. Mechatronics*, vol. 20, no. 2, pp. 812–823, Apr. 2015.

[8] R. Xu, X. Zhang, H. Guo, and M. Zhou, "Sliding mode tracking control with perturbation estimation for hysteresis nonlinearity of piezo-actuated stages," *IEEE Access*, vol. 6, pp. 30617–30629, 2018.

[9] J. Liu and K. Zhou, "Active vibration control of a dynamic hysteresis system using μ-synthesis," *IEEE Access*, vol. 6, pp. 76831–76837, 2018.

[10] X. Zhang, S. Su, G. Zhu, and Y. Peng, "Adaptive discrete-time estimated inverse control for piezoelectric positioning stage," *IEEE Access*, vol. 7, pp. 155120–155129, 2019.

[11] Y. Liu, J. Shan, and U. Gabbert, "Feedback/feedforward control of hysteresis-compensated piezoelectric actuators for high-speed scanning applications," *Smart Mater. Struct.*, vol. 24, no. 1, Nov. 2014, Art. no. 015012.

[12] J. Shan, Y. Liu, U. Gabbert, and N. Cui, "Control system design for nanopositioning using piezoelectric actuators," *Smart Mater. Struct.*, vol. 25, no. 2, Jan. 2016, Art. no. 025024.

[13] J. A. Mynderse and G. T.-C. Chiu, "Two-degree-of-freedom hysteresis compensation for a dynamic mirror actuator," *IEEE/ASME Trans. Mechatronics*, vol. 21, no. 1, pp. 29–37, Feb. 2016.

[14] Z. Li, J. Shan, and U. Gabbert, "Development of reduced Preisach model using discrete empirical interpolation method," *IEEE Trans. Ind. Electron.*, vol. 65, no. 10, pp. 8072–8079, Oct. 2018.

[15] Z. Li, J. Shan, and U. Gabbert, "Inverse compensator for a simplified discrete Preisach model using model-order reduction approach," *IEEE Trans. Ind. Electron.*, vol. 66, no. 8, pp. 6170–6178, Aug. 2019.

[16] I. MacKenzie and D. Trumper, "Real-time hysteresis modeling of a reluctance actuator using a sheared-hysteresis-model observer," *IEEE/ASME Trans. Mechatronics*, vol. 21, no. 1, pp. 4–16, Feb. 2016.

[17] G.-Y. Gu, C.-X. Li, L.-M. Zhu, and C.-Y. Su, "Modeling and identification of piezoelectric-actuated stages cascading hysteresis nonlinearity with linear dynamics," *IEEE/ASME Trans. Mechatronics*, vol. 21, no. 3, pp. 1792–1797, Jun. 2016.

[18] J. Zhang, D. Torres, J. L. Ebel, N. Sepulveda, and X. Tan, "A composite hysteresis model in self-sensing feedback control of fully integrated VO_2 microactuators," *IEEE/ASME Trans. Mechatronics*, vol. 21, no. 5, pp. 2405–2417, Oct. 2016.

[19] D. Pesotski, H. Janocha, and K. Kuhnen, "Adaptive compensation of hysteretic and creep non-linearities in solid-state actuators," *J. Intell. Mater. Syst. Struct.*, vol. 21, no. 14, pp. 1437–1446, Sep. 2010.

[20] Q. Yang and S. Jagannathan, "Creep and hysteresis compensation for nanomanipulation using atomic force microscope," *Asian J. Control*, vol. 11, no. 2, pp. 182–187, Mar. 2009.

[21] D. D. Rizos and S. D. Fassois, "Friction identification based upon the LuGre and Maxwell slip models," *IEEE Trans. Control Syst. Technol.*, vol. 38, no. 1, pp. 548–553, Jan. 2009.

[22] M. Goldfarb and N. Celanovic, "Modeling piezoelectric stack actuators for control of micromanipulation," *IEEE Control Syst. Mag.*, vol. 17, no. 3, pp. 69–79, Jun. 1997.

[23] Y. Liu, J. Shan, U. Gabbert, and N. Qi, "Hysteresis and creep modeling and compensation for a piezoelectric actuator using a fractional-order maxwell resistive capacitor approach," *Smart Mater. Struct.*, vol. 22, no. 11, Oct. 2013, Art. no. 115020.

[24] Y. Liu, J. Shan, Y. Meng, and D. Zhu, "Modeling and identification of asymmetric hysteresis in smart actuators: A modified MS model approach," *IEEE/ASME Trans. Mechatronics*, vol. 21, no. 1, pp. 38–43, Feb. 2015.
[25] H. Janocha and K. Kuhnen, "Real-time compensation of hysteresis and creep in piezoelectric actuators," *Sens. Actuators A, Phys.*, vol. 79, no. 2, pp. 83–89, Feb. 2000.
[26] B. Mokaberi and A. A. G. Requicha, "Compensation of scanner creep and hysteresis for AFM nanomanipulation," *IEEE Trans. Autom. Sci. Eng.*, vol. 5, no. 2, pp. 197–206, Apr. 2008.
[27] Y. Liu, J. Shan, and N. Qi, "Creep modeling and identification for piezoelectric actuators based on fractional-order system," *Mechatronics*, vol. 23, no. 7, pp. 840–847, Oct. 2013.
[28] M. Rakotondrabe, C. Clevy, and P. Lutz, "Hinf deflection control of a unimorph piezoelectric cantilever under thermal disturbance," in *Proc. IEEE/RSJ Int. Conf. Intell. Robots Syst.*, 2007, pp. 1–8.
[29] D. Habineza, M. Zouari, M. Hammouche, Y. L. Gorrec, and M. Rakotondrabe, "Characterization and modeling of the temperature effect on the piezoelectric tube actuator," *IFAC-PapersOnLine*, vol. 49, no. 21, pp. 354–360, 2016.
[30] M. B. Rauls, W. Dong, J. E. Huber, and C. S. Lynch, "The effect of temperature on the large field electromechanical response of relaxor ferroelectric 8/65/35 PLZT," *Acta Mater.*, vol. 59, no. 7, pp. 2713–2722, Apr. 2011.
[31] W. D. Dong, J. C. Valadez, J. A. Gallagher, H. R. Jo, R. Sahul, W. Hackenberger, and C. S. Lynch, "Pressure, temperature, and electric field dependence of phase transformations in niobium modified 95/5 lead zirconate titanate," *J. Appl. Phys.*, vol. 117, no. 24, Jun. 2015, Art. no. 244104.
[32] M. Rakotondrabe and I. A. Ivan, "Development and dynamic modeling of a new hybrid thermopiezoelectric microactuator," *IEEE Trans. Robot.*, vol. 26, no. 6, pp. 1077–1085, Dec. 2010.
[33] M. Rakotondrabe, M. C. Diouf, and P. Lutz, "Robust feedforward-feedback control of a hysteretic piezocantilever under thermal disturbance," *IFAC Proc. Volumes*, vol. 41, no. 2, pp. 13725–13730, 2008.
[34] R. Köhler and S. Rinderknecht, "A phenomenological approach to temperature dependent piezo stack actuator modeling," *Sens. Actuators A, Phys.*, vol. 200, no. 4, pp. 123–132, Oct. 2013.

YANFANG LIU received the B.Sc. degree in aircraft design and engineering from Harbin Engineering University, China, in 2008, and the Ph.D. degree in aeronautical and astronautical science and technology from the Harbin Institute of Technology, China, in 2014.

Since 2014, he has been a Lecturer with the Harbin Institute of Technology, China, where he is currently an Associate Professor with the Department of Aerospace Engineering, School of Astronautics. His research interests include smart materials and structures, nano-positioning, vibration isolation, unmanned aerial vehicles, and artificial intelligence.

NAIMING QI received the Ph.D. degree in precision instruments and machinery from the Harbin Institute of Technology, China, in 2001.

He is currently a Professor with the Department of Aerospace Engineering, School of Astronautics, Harbin Institute of Technology. His research interests include intelligent control, dynamics and control of spacecraft, and electromechanics.

ZHI LI received the Ph.D. degree in mechanical engineering from Concordia University, Canada, in 2015.

He was a Postdoctoral Research Fellow with the Eindhoven University of Technology, The Netherlands, and York University, Canada. He was an Alexander von Humboldt Research Fellow with Otto-von-Guericke Universität Magdeburg, Magdeburg, Germany. He is currently a Full Professor with the State Key Laboratory of Synthetical Automation for Process Industries, Northeastern University, Shenyang, China. His research interests include dynamics and control of smart actuators and hysteresis modeling and compensation.